

FEBRUARY 01 1972

# Numerical Study of Sound Refraction by a Jet Flow. I. Ray Acoustics

L. K. Schubert



*J. Acoust. Soc. Am.* 51, 439–446 (1972)

<https://doi.org/10.1121/1.1912861>



 **ASA**

Advance your science and career as a member of the **Acoustical Society of America**

[LEARN MORE](#)

# Numerical Study of Sound Refraction by a Jet Flow. I. Ray Acoustics

L. K. SCHUBERT\*

*University of Toronto Institute for Aerospace Studies, Toronto, Ontario, Canada*

Sound rays are traced numerically from a point source on the axis of a jet flow with realistically chosen velocity profiles. The directivity patterns computed from the ray paths have no cone of absolute silence, in contrast with analytic results for nonspreading jets. A related observation is that the surfaces of constant phase are ultimately spherical. Nevertheless, the computed axial refraction valleys are much deeper than those observed in jet noise studies. The difference is due to diffraction, which tends to offset refraction effects at all but the highest (ray-acoustic) frequencies.

## INTRODUCTION

In 1963 a series of experiments was begun in the anechoic chamber of the Institute for Aerospace Studies to investigate the farfield directivity pattern of a "point" source of sound immersed in a subsonic jet flow.<sup>1-5</sup> The observed patterns showed the same pronounced axial intensity minimum that is characteristic of aerodynamic jet noise. This similarity lent strong support to the view<sup>6-9</sup> that the downstream "valley" in jet noise is due to refraction rather than to the inherent directivity of the sound generated within the region of turbulence.

The success of the experiments inspired an attempt to verify the refraction interpretation analytically and at the same time to extend the available data. The first result of this attempt was a study of refraction at the high-frequency limit by ray-tracing methods. This work is reported here. The treatment of the more general wave-acoustics case is left to a second paper (Part II, pp. 447-463).

The source-jet configuration is shown in Fig. 1. The functions simulating the axial and transverse profiles of the mean velocity and temperature have been realistically chosen (Appendix A; see also Ref. 10, where the match with experimental data is shown graphically). This distinguishes the present work from calculations based on nonspreading flows in which the velocity is a function of the transverse coordinate only. Such idealized models predict complete silence far downstream of the source at all frequencies.<sup>11-13</sup> According to the results herein, the depth of the axial refraction

valley for a spreading jet remains finite even at the high-frequency limit.

The discussion below begins with a derivation of simple expressions describing the farfield phase and amplitude along the jet axis. Though based on geometrical acoustics, these results are valid for all frequencies.

Two numerical ray-tracing methods are then outlined which provide detailed high-frequency results. In the first method ("batch ray tracing") a 180° fan of rays and the corresponding wavefront are traced simultaneously in small time steps. The method is attractive because of its simplicity but breaks down in regions where rays intersect. In such regions each ray may be traced separately ("single ray tracing") by integration of its differential equation. Once the ray paths are known, the acoustic pressure can be estimated from the proximity of neighboring rays.

For comparison purposes the geometrical acoustics for an infinite cylindrical jet are given in Appendix B.

## I. FARFIELD PHASE AND AMPLITUDE ALONG JET AXIS

No matter how large the wavelength of the sound radiated by a source near the jet nozzle, the cross section of the flow is eventually much larger (and velocity gradients correspondingly small). Thus ray acoustics becomes applicable at arbitrary frequencies at points sufficiently remote from the nozzle.

The axial phase retardation relative to quiescent conditions (or relative to conditions at  $\theta=90^\circ$ ) at some large distance  $x_1$  downstream from the source is

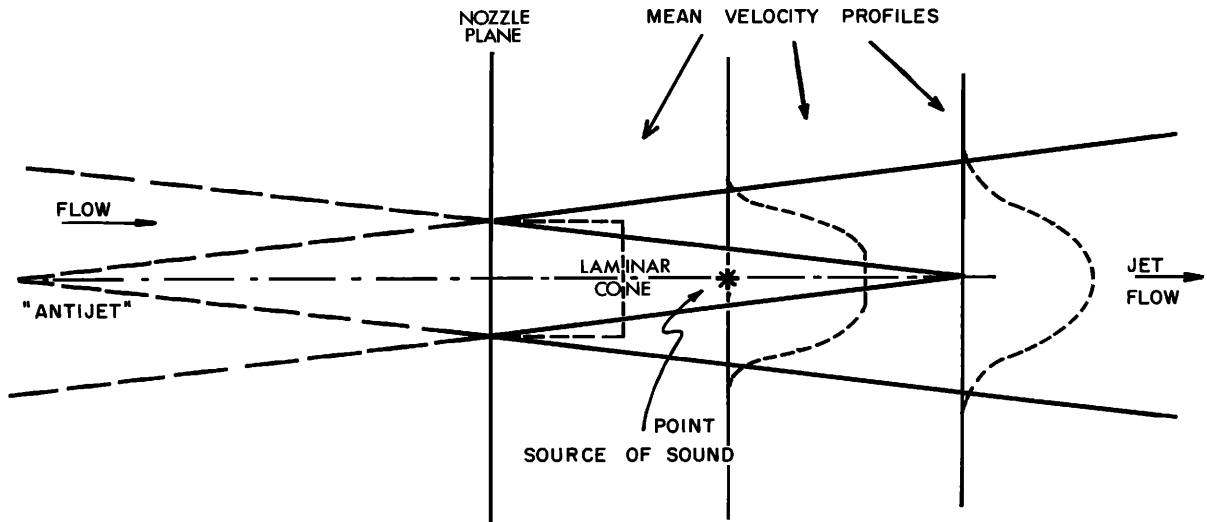


FIG. 1. Source-jet configuration. For explanation of "antijet" see Appendix A.

therefore

$$\begin{aligned} \phi_{\theta_0} - \phi_0 &\approx \omega \left[ \frac{x_1}{a_0} - \int_{x_0}^{x_1} \frac{dx_1}{(a+U)_{\text{axis}}} \right] \\ &\approx C_1 + \frac{\omega C_2}{a_0} \left( M_j C + \frac{C^2 - 1}{2} \right) \ln x_1, \end{aligned} \quad (1)$$

assuming that the ratio of axial-flow speed to jet-exit-flow speed is  $U_{\text{axis}}/U_j \approx C_2/x_1$  and  $a_{\text{axis}} - a_0^2 \approx C_2(a_j^2 - a_0^2)/x_1$ ;  $\omega$  is the radian source frequency,  $a_0$  and  $a_j$  are the ambient and jet exit sound speeds, respectively;  $M_j = U_j/a_j$ ,  $C = a_j/a_0$ , and  $C_2 = 6.39$  when distances are measured in multiples of the nozzle diameter  $D$ . The choice of the lower limit of integration  $x_0$  is unimportant for our purposes, as it merely affects the constant  $C_1$  and not the variation of phase in the limit of large  $x_1$ . It is evident from this formula that the axial phase differential increases forever. However, the ratio of the differential to  $x_1$  approaches zero, so that constant phase surfaces of increasing radius become more and more nearly spherical.

The axial-intensity variation far from the source can be determined from the following low-Mach-number version of a ray equation derived later on (Eq. 11,

with  $a = a_0 = \text{const}$ ):

$$d^2x_2/dx_1^2 = -a_0^{-1} \partial U / \partial x_2 + O(M^2), \quad (2)$$

where  $x_1$  and  $x_2$  are measured parallel and transverse to the jet axis, respectively. Restricting attention to rays very close to the jet axis, one can write  $\partial U / \partial x_2$  as  $-1195 U_j D x_2 x_1^{-3}$ , where the numerical constant is based on the analytical approximations to the flow field (Appendix A). Then the approximate solution of Eq. 2 is

$$x_2 = -C_3 \sum_{n=0}^{\infty} \frac{v^n}{n!(n+1)!} \int_{v_0}^v \left[ v \sum_{m=0}^{\infty} \frac{v^m}{m!(m+1)!} \right]^{-2} dv, \quad (3)$$

where  $v = 1195 M_j D / x_1$ . For sufficiently large  $x_1$  this becomes

$$x_2 \approx C_3 (v^{-1} + \ln v), \quad x_1 > 10^4 M_j D, \quad (4)$$

which gives the asymptotic variation of ray tube radius with axial distance. Although Eq. 3 is probably accurate for values of  $x_1$  as small as  $50 M_j D$ , its sensitivity to the

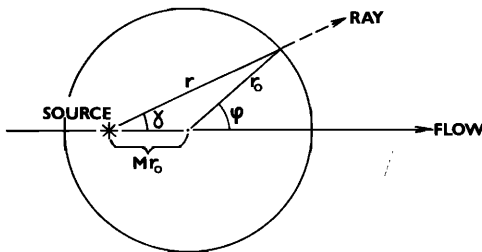


FIG. 2. Initial wavefront.

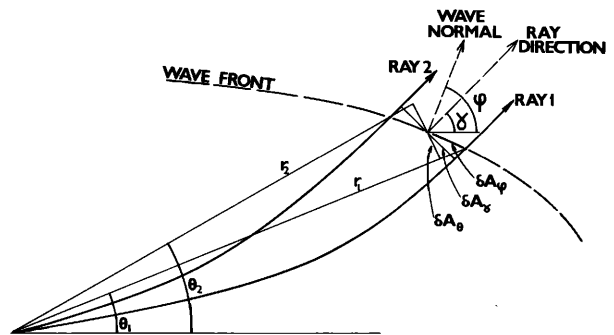


FIG. 3. Area relationships on a small section of a wavefront.

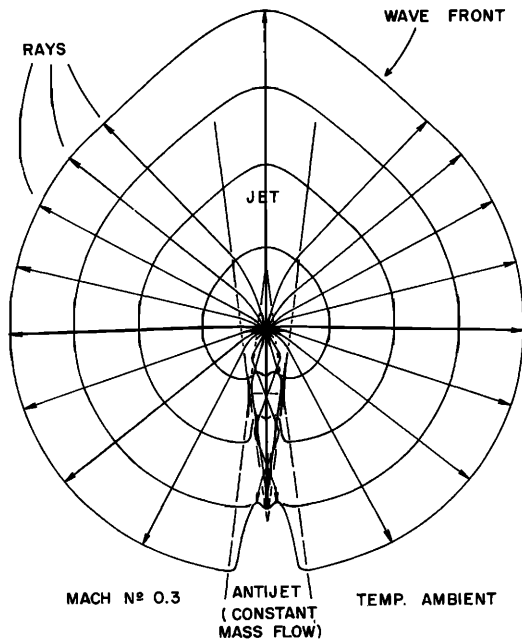


FIG. 4. Ray tracing. Downstream rays traced by "batch ray tracing" method, upstream rays traced individually. The wavefront is shown at intervals of  $1.5 \times 10^{-4} D$  sec, where  $D$  is the nozzle diameter in inches. The rays are equally spaced at the source, at  $15^\circ$  intervals (the ray emitted upstream at an angle of  $135^\circ$  has been omitted to avoid confusion; like the rays at  $150^\circ$  and  $165^\circ$  it is "trapped" by the anti-jet).

parameter  $v_0$  limits its usefulness at all but very great distances. From Eq. 4 the asymptotic axial sound pressure level (SPL), relative to that at  $\theta=90^\circ$ , is found to be

$$SPL_0^\circ - SPL_{90^\circ} \approx -C_4 + 10370(M_j D/x_1) \times \ln[x_1/(1195M_j D)], \quad x_1 > 10^4 M_j D. \quad (5)$$

Therefore the depth of the refraction valley approaches a constant at all frequencies. The effect of nonambient sound speed in the jet is to add further terms proportional to  $x_2 x_1^{-3}$  to Eq. 2, so that this conclusion holds for all jet speeds and temperatures.

### II. BATCH RAY TRACING

In the batch ray tracing method a fan of up to 33 rays distributed from  $\theta=0^\circ$  to  $\theta=180^\circ$  was jointly incremented in small time steps. Their termini at any instant define points on a wavefront. The ray increments were computed in accordance with the principle that the ray velocity is the vector sum of the sound velocity directed along the wave normal and the fluid flow velocity (e.g., Ref. 14).

Thus the slope of the wave normal at each ray terminus was required. If  $(r_1, \theta_1)$ ,  $(r_2, \theta_2)$ ,  $\dots$ ,  $(r_5, \theta_5)$  are the polar coordinates of five neighboring ray termini with respect to the source point on the jet axis, the slope of the wave normal for the third (central)

ray is found to be

$$[(r_3/r_3') \tan \theta_3 - 1]/(\tan \theta_3 + r_3/r_3'), \quad (6)$$

where

$$r_3' \approx \sum_{\substack{i=1 \\ i \neq 3}}^5 [(\prod_{\substack{j=1 \\ j \neq 3, i}}^5 K_{3j})(r_i - r_3)/(\prod_{\substack{j=1 \\ j \neq i}}^5 K_{ij})]$$

(with  $K_{ij} = \theta_i - \theta_j$ ) to an accuracy  $K_{31}K_{32}K_{34}K_{35}r^{(5)}(\bar{\theta})/5!$ .  $r_3'$  stands for the derivative  $dr/d\theta$  along the wavefront (at  $r_3, \theta_3$ ) and the above approximation is based on a quartic polynomial interpolated through the five ray termini. Mirror-image rays were used to complete groups of five rays near the axis.

### III. SINGLE RAY TRACING

Consider a ray in a plane containing the jet axis. The ray direction and wave-normal direction make angles  $\gamma$  and  $\varphi$  with the jet axis, respectively.

The generalized Snell's Law can be written as<sup>15</sup>

$$\frac{d}{ds} \left( \frac{\cos \varphi}{a + U \cos \varphi} \right) = -\frac{1}{V_s} \frac{1}{a + U \cos \varphi} \left( \frac{\partial a}{\partial x_1} + \cos \varphi \frac{\partial U}{\partial x_1} \right), \quad (7)$$

where  $a$  is the local sound speed,  $U$  the local flow speed (assumed parallel to  $x_1$ ),  $s$  the distance along the ray, and  $V_s$  the ray velocity  $= a(1 + 2M \cos \varphi + M^2)^{1/2} = a[M \times \cos \gamma + (1 - M^2 \sin^2 \gamma)^{1/2}]$ , with  $M = U/a$ . Note that

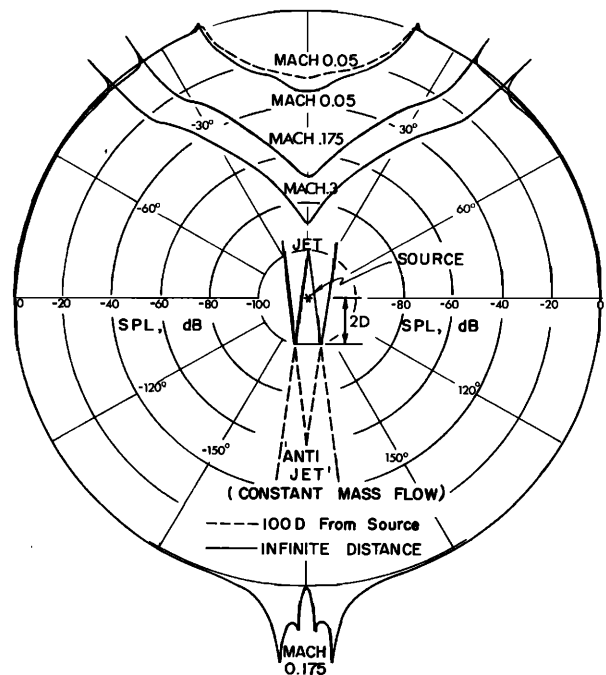


FIG. 5. High-frequency limit of the directivity patterns. Method: single ray tracing, with downstream data verified by batch ray tracing.

the right-hand side of Eq. 7 vanishes for a stratified medium, which is a frequently used approximation. Carrying out the differentiation and substituting

$$\frac{d}{ds} \equiv \cos\gamma \frac{\partial}{\partial x_1} + \sin\gamma \frac{\partial}{\partial x_2}; \tag{8}$$

$$\cos\gamma = \frac{U + a \cos\varphi}{V_s}; \quad \sin\gamma = \frac{a \sin\varphi}{V_s},$$

one finds

$$\frac{d\varphi}{ds} = \frac{1}{V_s} \left[ \sin\varphi \frac{\partial a}{\partial x_1} - \cos\varphi \frac{\partial a}{\partial x_2} + \cos\varphi \left( \sin\varphi \frac{\partial U}{\partial x_1} - \cos\varphi \frac{\partial U}{\partial x_2} \right) \right]. \tag{9}$$

To obtain an expression for the curvature  $d\gamma/ds$  of the ray, one may differentiate  $\tan\gamma = \sin\varphi/(M + \cos\varphi)$  with respect to  $s$ .

This yields

$$\frac{d\gamma}{ds} = \frac{a^2}{V_s^2} \left[ (1 + M \cos\varphi) \frac{d\varphi}{ds} - \sin\varphi \frac{dM}{ds} \right]. \tag{10}$$

Substituting  $d\varphi/ds$  from Eq. 9 and using Eq. 8 one obtains, after slight reduction, gives

$$\begin{aligned} \frac{d\gamma}{ds} = \frac{1}{V_s} \left\{ \sin\varphi \frac{\partial a}{\partial x_1} - \frac{a^2}{V_s^2} \left[ (\cos\varphi + 2M \cos^2\varphi - M) \frac{\partial a}{\partial x_2} \right. \right. \\ \left. \left. + M \sin^3\varphi \frac{\partial U}{\partial x_1} + (1 + M \cos^3\varphi) \frac{\partial U}{\partial x_2} \right] \right\} \\ = \frac{1}{V_s} \left\{ \frac{V_s}{a} \sin\gamma \frac{\partial a}{\partial x_1} + \left( 2M \sin^2\gamma - \frac{a}{V_s} \cos\gamma \right) \frac{\partial a}{\partial x_2} \right. \\ \left. - \frac{V_s}{a} M \sin^3\gamma \frac{\partial U}{\partial x_1} \right. \\ \left. - \frac{a^2}{V_s^2} \left[ 1 + M \left( \frac{V_s}{a} \cos\gamma - M \right)^3 \right] \frac{\partial U}{\partial x_2} \right\}. \tag{11} \end{aligned}$$

An explicit differential equation for a ray may be obtained from Eq. 11 by expressing the trigonometric ratios of  $\gamma$  in terms of  $dx_2/dx_1$  and noting that  $d\gamma/ds = d^2x_2/dx_1^2 [1 + (dx_2/dx_1)^2]^{-1/2}$ . Alternatively, one may employ Eq. 11 directly for numerical ray tracing, since it specifies the curvature of a ray for a given position and inclination. One proceeds in circular arcs small enough to accommodate the local rate of change of curvature and large enough to prevent the accumulation of appreciable roundoff error.

IV. EVALUATION OF SOUND-PRESSURE LEVEL

To estimate the SPL from ray-tracing results, one first computes the acoustic intensity between two nearby ray cones (whose vertices coincide with the point source on the jet axis):

$$I = e/\delta A_\gamma. \tag{12}$$

Here  $e$  is the constant energy flow between two ray cones and  $\delta A_\gamma$  is the component of the intercepted area normal to the ray direction. Once  $I$  is known, the SPL can be computed from the energy formula appropriate to a moving medium<sup>14,16</sup>:

$$I = \frac{\bar{p}^2 V_f V_s}{\rho a^3} = \frac{\bar{p}^2 (1 + M \cos\varphi) (1 + 2M \cos\varphi + M^2)^{1/2}}{\rho a}, \tag{13}$$

where  $\bar{p}^2$  is the mean-square sound pressure, and  $V_f$  and  $V_s$  are the magnitudes of the phase velocity and ray velocity, respectively.

The energy flow  $e$  in Eq. 12 can be calculated by considering a small spherical wavefront of radius  $r_0$  which has originated at the point source in the laminar cone.<sup>17</sup>

Referring to Fig. 2,

$$\begin{aligned} (r/r_0)^2 &= 1 + 2M \cos\varphi + M^2; \\ \sin\gamma &= (r_0/r) \sin\varphi; \end{aligned} \tag{14}$$

$$\cos\gamma = (r_0/r) (M + \cos\varphi);$$

$$\cos(\varphi - \gamma) = (1 - M^2 \sin^2\gamma)^{1/2} = (r_0/r) (1 + M \cos\varphi).$$

Thus the pressure at high frequencies, for source strength  $s_0$ ,<sup>13,14</sup>

$$\begin{aligned} p(r, \gamma, t) \approx \frac{(1 - M^2 \sin^2\gamma)^{1/2} - M \cos\gamma}{(1 - M^2)(1 - M^2 \sin^2\gamma)} \frac{s_0}{4\pi r} \\ \times \exp \left\{ -i\omega \left[ t - \frac{r (1 - M^2 \sin^2\gamma)^{1/2} - M \cos\gamma}{1 - M^2} \right] \right\}, \tag{15} \end{aligned}$$

can be written as

$$p(r_0, \varphi, t) \approx \frac{1}{(1 + M \cos\varphi)^2} \frac{s_0}{4\pi r_0} \exp \left[ -i\omega \left( t - \frac{r_0}{a} \right) \right]. \tag{16}$$

Now the energy flowing between two ray cones can be found by integrating the intensity over the portion of the wavefront lying between the ray cones, i.e.,

$$\begin{aligned} e &= \int_A \mathbf{I} \cdot d\mathbf{A} = \int_A I \cos(\varphi - \gamma) dA \\ &= \frac{s_0^2}{16\pi\rho a} \int_{\varphi_1}^{\varphi_2} \frac{\sin\varphi d\varphi}{(1 + M \cos\varphi)^2} \quad (\text{from Eqs. 13, 14, 16}) \\ &= \frac{s_0^2}{16\pi\rho a} \frac{1}{M} \left[ \frac{1}{(1 + M \cos\varphi_2)} - \frac{1}{(1 + M \cos\varphi_1)} \right]. \tag{17} \end{aligned}$$

To evaluate Eq. 12, it remains to compute  $\delta A_\gamma$  from the ray paths.

From Fig. 3 it is apparent that

$$\begin{aligned} \delta A_\gamma &\approx \delta A_\varphi \cos(\varphi - \gamma) \\ \delta A_\varphi &\approx \delta A_\theta / \cos(\varphi - \theta) \\ \delta A_\theta &\approx 2\pi r^2 \sin\theta \delta\theta \approx 2\pi r^2 (\cos\theta_1 - \cos\theta_2), \end{aligned}$$

so that

$$\delta A_\gamma \approx 2\pi r^2 (\cos\theta_1 - \cos\theta_2) \cos(\varphi - \gamma) / \cos(\varphi - \theta). \quad (18)$$

Equations 12, 13, 17, and 18 may be combined to give the SPL (see Ref. 18):

$$\text{SPL}(r, \theta) \approx \text{const} + 10 \log_{10} \left[ \frac{1}{ar^2} \frac{\cos\varphi_1' - \cos\varphi_2'}{\cos\theta_1 - \cos\theta_2} \frac{\cos(\varphi - \theta)}{(1 + M' \cos\varphi_1')(1 + M' \cos\varphi_2')(1 + M \cos\varphi)^2} \right], \quad (19)$$

where primed quantities refer to conditions on the initial wavefront, and unsubscripted variables represent averages for rays 1 and 2.

When rays intersect, this formula fails. Approximate farfield intensities may, however, be obtained as follows. Initially space the rays so that the same energy flow is associated with each ray cone. Then trace each ray until it suffers no further deflection. If the final ray angles of two ultimately neighboring rays are  $\gamma_1$  and  $\gamma_2$ , then sufficiently far from the flow the intensity at  $\gamma = (\gamma_1 + \gamma_2)/2$  will be approximately proportional to  $r^{-2}(\cos\gamma_1 - \cos\gamma_2)^{-1}$ .

V. RESULTS AND CONCLUDING REMARKS

Some results of "batch ray tracing" and "single ray tracing" are shown in Figs. 4-7.<sup>19</sup> As anticipated from

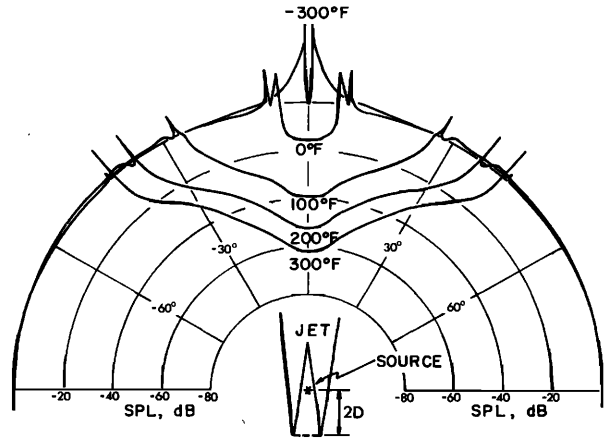


FIG. 6. Single ray tracing results for heated and cooled jets. Mach No.  $M_j = 0.05 a_0/a_j$  (constant speed). Observer distance  $= \infty$ .

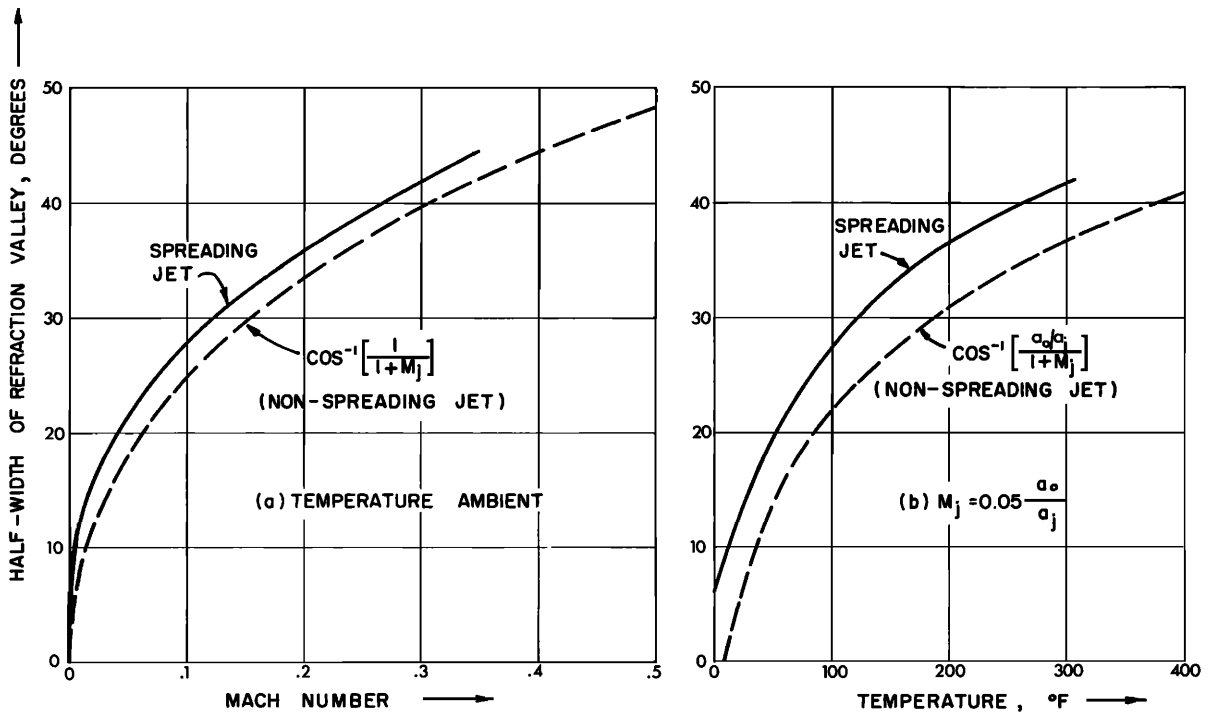


FIG. 7. Width of refraction valley in ray-acoustic limit for spreading and nonspreading jet. (a) Unheated jet and (b) hot jet.

16 June 2024 19:52:47

Sec. I there are no cones of complete silence. However, the edges of the refraction valleys are sharply defined and the valleys are very deep (89 dB at Mach 0.3). The variation in the width of the valley with Mach number and temperature is very similar to that computed for a nonspreading jet (Appendix B). The depth of the valley approaches its asymptotic farfield value very slowly as the distance from the source increases. Even beyond  $100D$  the valley deepens by as much as 5, 9.5, and 18.2 dB for Mach 0.05, 0.175, and 0.3 jets, respectively. The numerical results are consistent with the prediction from Eq. 5 that the valley depth should change by about 2 dB beyond  $10^4 M_j D$ .

Comparison with experimental results<sup>1-5</sup> immediately shows that the valley depth computed by ray acoustics greatly exceeds measured values at typical jet-noise frequencies (e.g., 71 dB at Mach 0.3 vs 7.3 dB measured at Mach 0.3,  $fD/U=0.37$ ). Thus, while the use of an axially decaying flow field assures nonzero intensity in the refraction valley, any attempt to delineate the refraction valley quantitatively at typical jet-noise frequencies must take into account diffractive scattering; that is, it must employ wave acoustics. Results from ray acoustics can, however, serve as an asymptotic check of wave acoustics results at the high-frequency limit.

**APPENDIX A: VELOCITY AND TEMPERATURE PROFILES**

The following summarizes the analytical approximations to the mean jet velocity ratio  $V(=U/U_j)$  used in the present work. Nondimensional distances  $\xi_1=x_1/D$ ,  $\xi_2=x_2/D$  are used.

- (1):  $V=1$ ,
- (2):  $V=1+0.017\{[(\xi_2-0.5)/\xi_1+0.125]/0.075\}^2 - 0.117\{[(\xi_2-0.5)/\xi_1+0.125]/0.075\}^3$ ,
- (3):  $V/V_{axis}=1+\left[\frac{4.2267}{\xi_1(0.5-0.05\xi_1)}-\frac{0.3}{(0.5-0.05\xi_1)^2}\right]\xi_2^2 + \left[\frac{0.2}{(0.5-0.05\xi_1)^3}-\frac{4.2267}{\xi_1(0.5-0.05\xi_1)^2}\right]\xi_2^3$ , (A1)
- (4):  $V/V_{axis}=\exp\{-52.65[(\xi_2-0.5)/\xi_1+0.0946]^2\}$ ,
- (5):  $V/V_{axis}=\exp\{-2.304[\xi_2/(0.5+0.1145\xi_1)]^2\}$ ,
- (6):  $V/V_{axis}=\exp\{-2.304[\xi_2/(0.16+0.157\xi_1)]^2\}$ ,
- (7):  $V/V_{axis}=0.3525-(2.204\xi_2-1.102)/\xi_1$ ,
- (8):  $V/V_{axis}=0.5608-0.4608\xi_2/(0.5+0.1145\xi_1)$ ,
- (9):  $V/V_{axis}=0.5608-0.4608\xi_2/(0.16+0.157\xi_1)$ ,

where

$$V_{axis}=1, \text{ for } \xi_1 \leq 4,$$

$$V_{axis}=\{0.21255+4.52 \times 10^{-5}\xi_1+[1.0117-0.19588\xi_1+(0.15645\xi_1)^2]^{1/2}\}^{-1}, \text{ for } \xi_1 > 4.$$

Note that sections of Gaussian curves have been used throughout the jet [regions (4), (5), and (6)].<sup>A1</sup> This is simpler and no less accurate than the more usual characterization of the flow profile by an error function in the mixing region ( $\xi_1 \leq 4$ ) and a rational function in the fully developed jet ( $\xi_1 \geq 8$ ) (see, e.g., Ref. 9). Some comparisons with measured profiles are made in Ref. 10.

Radial velocity components have been neglected in

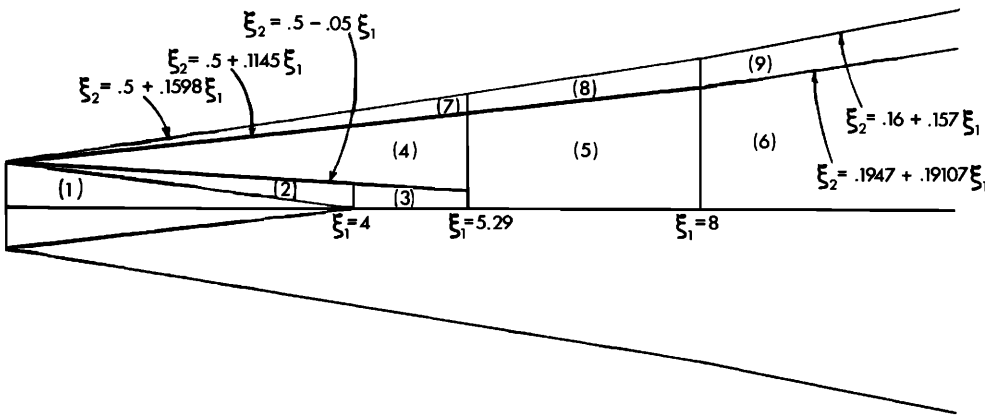


FIG. A-1. Subdivision of jet flow field for analytical approximations.

the flow model, since they are nearly two orders of magnitude smaller than the jet centerline velocity.

According to Ref. A2, the normalized temperature ratio  $T = (a^2 - a_0^2)/(a_0^2 - a_0'^2)$  is proportional to the velocity ratio  $V = U/U_j$  on the jet axis and proportional to  $V^{\frac{1}{2}}$  transverse to it. It follows that the local temperature ratio and sound speed are given by

$$T(\xi_1, \xi_2) = [V(\xi_1, \xi_2) V(\xi_1, 0)]^{\frac{1}{2}} \quad (\text{A2})$$

and

$$a = a_0 [1 + (a_j^2/a_0^2 - 1)T]^{\frac{1}{2}}.$$

The "antijet" appearing in Figs. 1, 4, and 5 is a fictitious convergent flow matching the emergent flow at the nozzle plane. Its main purpose was to facilitate the later wave-acoustic approach; in the present context it helps to indicate the effects of acoustic "channeling" or focusing.

### APPENDIX B: RAY ACOUSTICS FOR NONSPREADING JET

For comparison with ray tracing results it is of interest to compute the directivity pattern for a source on the axis of an infinite axisymmetric cylindrical flow.

Making use of the law of energy conservation in a ray tube,<sup>14</sup> one can express the pressure  $p$  outside the flow in terms of the pressure  $p'$  on the initial wavefront (with radius  $r_0$ ) as (cf. Csanady<sup>B1</sup>)

$$\bar{p}^2 = \frac{\rho_0 a_0 V_s'}{\rho' a'} (1 + M' \cos \varphi') \frac{dS'}{dS} \bar{p}'^2, \quad (\text{B1})$$

where  $dS$  is the cross-sectional area of the ray tube. A great distance  $r$  from the source

$$\frac{V_s' dS'}{a' dS} \approx (1 + M' \cos \varphi') \frac{r_0^2 \sin \varphi' d\varphi'}{r^2 \sin \varphi d\varphi}, \quad (\text{B2})$$

where the approximation  $dS \approx r d\varphi \cdot r \sin \varphi d\Omega$  (see Fig. B-1) has been used.

This approximation breaks down for  $\varphi' = 0$  and hence for all  $\varphi$  smaller than or equal to the minimum angle of emergence because the ray then travels down the axis of the flow.<sup>B2</sup> The minimum angle of emergence is  $\varphi = \cos^{-1}[a_0/(a' + U')]$ , obtained by setting  $\varphi'$  to zero in the stratified-medium law of ray propagation (e.g., see Ref. 14 or Eq. 7)

$$\frac{1}{a'} \frac{\cos \varphi'}{1 + M' \cos \varphi'} = \frac{1}{a_0} \cos \varphi. \quad (\text{B3})$$

Equation B3 may be used to eliminate  $\varphi'$  from Eqs. B1 and B2, giving

$$\bar{p}^2 = (\rho_0/\rho) (a_0/a')^4 (r_0/r)^2 (a_0/a' - M' \cos \varphi)^{-4} \bar{p}'^2 \quad (\text{B4})$$

for  $\varphi > \cos^{-1}[a_0/(a' + U')]$ . This is valid for arbitrary pressures  $p'$  on the initial wavefront. It follows from

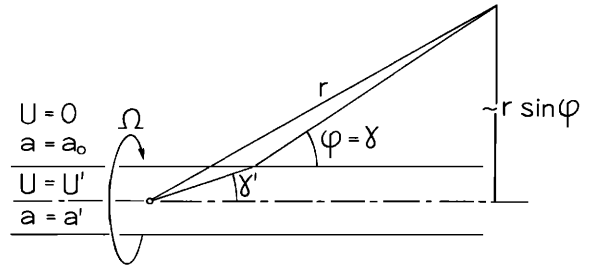


FIG. B-1. Approximation for ray from stratified flow.

Eq. 16 that  $r_0^2 \bar{p}'^2 \propto (1 + M' \cos \varphi')^{-4}$  for a simple stationary source, and by Eq. B3 this equals  $(a_0/a')^{-4} \times (a_0/a' - M' \cos \varphi)^4$ . Thus Eq. B4 becomes simply

$$\bar{p}^2 \propto 1/r^2 \quad (\text{B5})$$

for a simple stationary source and for  $\varphi > \cos^{-1}[a_0/(a' + U')]$ , i.e., the directivity beyond the minimum angle of emergence is perfectly omnidirectional. However, the intensity is  $(1 - M'^2)a'/a_0$  times the intensity for a simple source radiating the same total power into still air (this may be verified from Eqs. 16, 17, and B4). When  $a_0/a' + M' > 1$ , rays trapped in the flow by total internal reflection travel upstream and produce a sharp spike in the farfield intensity at  $\varphi = \pi$ . This accounts for a fraction  $(1 + M')(1 - a'/a_0 + a'M'/a_0)/2$  of the total power "missing" from the remainder of the pattern.<sup>B3</sup> For  $a_0/a' > 1 + M'$ , trapped energy travels both upstream and downstream and there is no refraction valley; for  $a_0/a' + M' < 1$  no energy is trapped and there are upstream and downstream refraction valleys.

Instead of a stationary simple source, Csanady<sup>B1</sup> considers an elemental volume containing quadrupoles moving with the flow speed and whose net radiation is omnidirectional in the moving frame, and finds

$$r_0^2 \langle \delta p'^2 \rangle_{av} \sim (1 + M' \cos \varphi')^{-1} = (a_0/a') (a_0/a' - M' \cos \varphi)^{-1}, \quad (\text{B6})$$

where the factor  $(1 + M' \cos \varphi')$  results from the apparent length contraction due to retarded time effects. In this case Eq. B4 becomes

$$\langle \delta p^2 \rangle_{av} \sim r^{-2} [1 - (U'/a_0) \cos \varphi]^{-5} \quad (\text{B7})$$

for  $\varphi > \cos^{-1}[a_0/(a' + U')]$ . This differs from the simple stationary source result, Eq. B5, by the factor  $[1 - (U'/a_0) \cos \varphi]^{-5}$ .

\* Present address: Department of Computing Science, University of Alberta, Edmonton 7, Alberta, Canada.

<sup>1</sup> J. Atvars, L. K. Schubert, and H. S. Ribner, J. Acoust. Soc. Amer. 37, 168-170 (1965).

<sup>2</sup> J. Atvars, L. K. Schubert, and H. S. Ribner, "Refraction of Sound from a Point Source Placed in an Air Jet," AIAA Aerospace Sci. Meeting, 2nd, New York, 25-27 Jan. 1965, AIAA Paper No. 65-82.

<sup>3</sup> E. Grande, J. Acoust. Soc. Amer. 38, 1063-1064 (1965).

<sup>4</sup> J. Atvars, L. K. Schubert, E. Grande, and H. S. Ribner, "Refraction of Sound by Jet Flow and Jet Temperature," NASA CR-494 (May 1966).

<sup>5</sup> E. Grande, "Refraction of Sound by Jet Flow and Jet Temperature II," Univ. Toronto Inst. Aerospace Studies, Tech. Note 110 (1966); also NASA CR-840 (Aug. 1967).

<sup>6</sup> A. Powell, "Survey of Experiments on Jet Noise," Aircraft Eng. 26, 2-9 (1954).

<sup>7</sup> H. S. Ribner, "Aerodynamics Sound from Fluid Dilatations—A Theory of the Sound from Jets and other Flows," Univ. Toronto Inst. Aerospace Studies, Rep. 86 (AFOSR TN 3430) (1962).

<sup>8</sup> H. S. Ribner, J. Acoust. Soc. Amer. 35, 614-616 (1963).

<sup>9</sup> H. S. Ribner, "The Generation of Sound by Turbulent Jets," Advan. Appl. Mech. 8, 103-182 (1964).

<sup>10</sup> L. K. Schubert, "Refraction of Sound by a Jet: A Numerical Study," Univ. Toronto Inst. Aerospace Studies, Tech. Note 144 (1969).

<sup>11</sup> H. S. Ribner, J. Acoust. Soc. Amer. 29, 435-441 (1957).

<sup>12</sup> P. Gottlieb, "Acoustics in Moving Media," PhD thesis, Physics Dept., MIT (1959); also J. Acoust. Soc. Amer. 32, 1117-1122 (1960).

<sup>13</sup> G. Moretti and S. Slutsky, "The Noise Field of a Subsonic Jet," Gen. Appl. Sci. Lab., GASL Tech. Rep. No. 150 (AFOSR TN-59-1310) (1959).

<sup>14</sup> D. I. Blokhintsev, "Acoustics of a Nonhomogeneous Moving Medium," in Russian (1946), translated by Natl. Adv. Comm. Aeron. NACA T.M. 1399 (1956).

<sup>15</sup> E. T. Kornhauser, "Ray Theory for Moving Fluids," J. Acoust. Soc. Amer. 25, 945-949 (1953). P. Uginčius, in J. Acoust. Soc. Amer. 37, 476-479 (1965), has derived a still more general equation valid for an arbitrary steady three-dimensional flow field.

<sup>16</sup> H. S. Ribner, "Note on Acoustic Energy Flow in a Moving Medium," Univ. Toronto Inst. Aerospace Studies, UTIAS TN21 (AFOSR TN 58-360, AD 15426) (1958).

<sup>17</sup> The results derived here can also be shown to be valid for a source downstream of the laminar cone, where the flow is nonuniform.

<sup>18</sup> Eqs. 17 and 19 correct Eqs. (A10) and (A15) of Ref. 10.

<sup>19</sup> The "antijet" is explained in Appendix A. Numerical accuracy was ensured by experimentation with various step sizes, ray densities, and computational precision.

<sup>20</sup> Suggested to the writer by W. T. Chu and T. E. Siddon.

<sup>21</sup> G. N. Abramovich, *The Theory of Turbulent Jets* (MIT Press, Cambridge, Mass., 1963).

<sup>22</sup> G. T. Csanady, "The Effect of Mean Velocity Variations on Jet Noise," J. Fluid Mech. 26, 183-197 (1966).

<sup>23</sup> In fact, the correct value of  $dS$ , assuming uniform  $U'$  in the flow region, is

$$\left\{ \frac{r'}{r} + \frac{D}{2r} \left( \frac{a_0}{a'} \sin \varphi \right)^2 \left[ \left( \frac{a_0}{a'} - M' \cos \varphi \right)^2 - \cos^2 \varphi \right]^{-1/2} \right\} \times \left( \frac{r'}{r} + \frac{D}{2r \sin \varphi} \right) r^2 \sin \varphi d\varphi d\Omega,$$

where

$$r'/r = [1 - (D/2r)^2 (\sin \varphi \cot \gamma' - \cos \varphi)^2]^{1/2} - (D/2r) \cos \varphi (\cot \gamma' - \cot \varphi)$$

and

$$\cot \gamma' = [(a_0/a')M' \sec \varphi + 1 - M'^2] \{ [(a_0/a') \sec \varphi - M']^2 - 1 \}^{-1/2}$$

which becomes complex for  $\varphi \leq \cos^{-1} [a_0/(a'+U')]$ .

<sup>24</sup> The "missing" power was incorrectly accounted for in Ref. 10.